

ORIGINAL RESEARCH ARTICLE

Cu/CuO/ZnO/PPy heterojunction material was prepared for Hg²⁺ anti-interference detection in seawater

Ming Li, Zhengming Li, Xiaotong Dong, Liangbin Jia, Meiyuan Zhu, Ye Ma, Minggang Zhao*, Hongzhi Cui

Department of Materials Science and Engineering, Ocean University of China, Qingdao 266100, China. E-mail: zhaomg@ouc.edu.cn

ABSTRACT

Hg²⁺ pollution poses a major threat to human health and the ecological environment, but there is still a lack of direct and sensitive Hg²⁺ detection technology. In this study, Cu/CuO/ZnO wires were prepared by alkaline oxidation and hydrothermal methods. Polypyrrole (PPy) was covered on the surface of the material by electrochemical polymerization. Using the principle of electrochemical signal response driven by p-n junction barrier, the material was used for the direct electrochemical detection of Hg²⁺ and was tested by differential pulse voltammetry. The composite has a good linear relationship in the Hg²⁺ concentration range of 200–1600 nmol/L, and has ultra-high sensitivity (1,010.82 $\mu\text{A}\cdot\text{L}/(\text{nmol}\cdot\text{cm}^2)$) and ultra-low detection limit (2.1 pmol/L). The new sensing mode based on the interface barrier eliminates the interference of other ions. The recovery rate of Hg²⁺ in tap water, river water and sea water is 97.3%–105.0%, and the RSD is 1.8%–5.6%. This method using p-n junction barrier can be extended to the development and research of other sensors for detecting heavy metal ions.

Keywords: P-n Junction; Mercury Ion; Interfacial Barrier; Electrochemical Detection; Metal Wire

ARTICLE INFO

Received: 24 August 2022
Accepted: 15 October 2022
Available online: 23 October 2022

COPYRIGHT

Copyright © 2022 Ming Li, *et al.*
EnPress Publisher LLC. This work is licensed under the Creative Commons Attribution-NonCommercial 4.0 International License (CC BY-NC 4.0).
<https://creativecommons.org/licenses/by-nc/4.0/>

1. Introduction

Mercury ion (Hg²⁺) can seriously damage organs and nervous system, leading to renal failure, cognitive and motor disorders, Minamata disease, etc.^[1,2]. Hg²⁺ pollutants are rich and highly toxic, and even low concentrations of Hg²⁺ will cause significant harm to human health and the ecological environment. The on-site quantitative detection method of Hg²⁺ is a research hotspot in related fields^[3]. There are a lot of interfering ions in actual water samples. Therefore, developing a convenient, fast and direct Hg²⁺ detection technology for the detection of Hg²⁺ in actual complex water bodies has important theoretical and practical application value.

At present, the detection methods of Hg²⁺ mainly include atomic absorption spectrometry, X-ray fluorescence spectrometry, inductively coupled plasma mass spectrometry, etc.^[4–6]. These methods have some disadvantages, such as expensive equipment, complex operation and unsuitable for on-site detection^[7,8]. Electrochemical detection method is widely used in the detection of metal ions because of its sensitive, fast and simple characteristics. Anodic stripping voltammetry (ASV) is an electrochemical analysis technology widely used in the detection of heavy metals, but it is not suitable for on-site detection because it requires a preconcentration step^[9]. At present, some electrochemical biosensors based on DNA or enzyme have been used to detect Hg²⁺^[10], but

strict operating conditions limit their application in actual water environment detection^[11]. In addition, since electrochemical analysis methods are usually based on redox reactions, substances with redox like properties will interfere with electrochemical detection. Therefore, eliminating the interference signal of such substances is also a challenge^[12].

The construction of semiconductor heterojunction shows unique advantages in different application fields such as photocatalysis, biosensor, photochemistry and electrocatalysis^[13–17]. Among them, p-n junction, which is composed of n-type and p-type semiconductors, is an important semiconductor heterojunction. The built-in electric field and interface energy barrier of p-n junction have adjustable characteristics, which can have a great impact on the movement of electrons^[18]. For example, the p-n junction is constructed by two organic semiconductors, perylene diimide derivative/poly (fluorene-co-phenylene), which promotes the generation and migration of electrons and holes, and realizes the efficient reduction of CO₂^[19]; ZnO/BiOI p-n junction can play a crucial role in improving the electrochemical biosensor performance of glucose^[20]. P-n junction can effectively adjust the electronic properties of materials, and has broad application prospects in the field of sensors.

CuO is a typical p-type semiconductor, which is widely used in catalysis, charge storage and other fields^[21,22]. ZnO is a wide band gap n-type semiconductor, which is widely used in photoelectric equipment, catalysis and other fields^[23,24]. CuO and ZnO can form typical p-n junctions with good conductivity and large barrier adjustment range^[25,26]. In addition, polypyrrole (PPy) as a conductive polymer, its NH functional group has high affinity for Hg²⁺, and the lone pair electrons on nitrogen coordinate with Hg²⁺ to form a stable complex, so it can specifically adsorb Hg²⁺^[27].

In this study, Cu/CuO/ZnO/PPy wires were prepared and applied to the direct electrochemical detection of Hg²⁺. PPy is used as the selective adsorption membrane of Hg²⁺ and the p-n barrier is used as the driving factor to change the electrochemical response, eliminating the interference of other ions. It has ultra-high sensitivity in the detec-

tion of Hg²⁺ in actual water samples. The results of this study show that using electrochemical interface barrier effect to directly detect heavy metal ions in the actual water environment is a method with good development prospects.

2. Experimental part

2.1 Instruments and reagents

Carl Zeiss AG-ULTRA 55 scanning electron microscope (Carl Zeiss AG, Germany); Ultima IV X-ray diffractometer (Nippon Science Co., Ltd.); Nicolet iS10 spectrophotometer, Thermo ESCALAB XI+ photoelectron spectrometer (Thermo Fisher Scientific, USA); CHI600E electrochemical workstation (Shanghai Chenhua Instrument Co., Ltd.).

Zn(CH₃COO)₂·2H₂O (Beijing Aladdin Holding Group Co., Ltd.); *N, N*-dimethylformamide (DMF, Shanghai McLean Biochemical Co., Ltd.). Other reagents were purchased from Sinopharm Chemical Reagent Co., Ltd. Phosphate buffer is prepared by mixing NaH₂PO₄·2H₂O and Na₂HPO₄·12H₂O in different proportions. All reagents used in this study are of analytical grade and do not need further purification. Copper wire ($\varphi = 0.5$ mm, Dongguan Rongyue Metal Materials Co., Ltd.).

2.2 Preparation of Cu/CuO wire

Cu(OH)₂ was synthesized by alkaline oxidation. Soak the cleaned copper wire in the mixed solution prepared with 1.413 g (N₂H₄)₂S₂O₈, 5 g NaOH and 50 mL deionized water for 5 minutes to grow Cu(OH)₂. When the surface of the copper wire turns light blue, blow the copper wire dry with nitrogen (N₂). The copper wire grown with Cu(OH)₂ was placed in an oven and maintained at a constant temperature for 3 hours at 180 °C. The surface of Cu(OH)₂ was observed to be blackened, which proved that it had been converted to CuO.

2.3 Preparation of Cu/CuO/ZnO wire

Dissolve 0.3 g Zn(CH₃COO)₂·2H₂O in 50 ml DMF and sonicate for 10 min. Then, the prepared Cu/CuO wire was added, and the solution was heated to 95 °C. After hydrothermal reaction for 7

hours, the color of the solution changed to white, and the raw material changed from black to gray white. The obtained gray Cu/CuO/ZnO was washed repeatedly with absolute ethanol and deionized water, dried in an oven at 60 °C and stored for standby.

2.4 Preparation of Cu/CuO/ZnO/PPy wire

The electrochemical polymerization of pyrrole monomer is to prepare 0.15 mol/L sodium dodecylbenzene sulfonate (SDBS) electrolyte with deionized water, and Electropolymer 0.1 mol/L pyrrole monomer with chronopotentiometry and three electrode system (Cu/CuO/ZnO wire as working electrode, Pt wire and Ag/AgCl electrode as counter electrode and reference electrode respectively). The voltage range is controlled at $-1-4$ V, and the current density of electropolymerization is 3 mA/cm^2 for 400 s. After deposition, wash the working electrode with deionized water and dry it in a vacuum oven at 60 °C for 6 hours.

2.5 Material characterization and electrochemical test

The size and microstructure of the prepared samples were characterized by Carl Zeiss AG-ULTRA 55 scanning electron microscope (SEM). We used Ultima IV X-ray diffractometer at a scanning speed of $10^\circ/\text{min}$ in the range of $2\theta = 5^\circ-80^\circ$, then, we obtained the X-ray diffraction (XRD) patterns of the samples. The samples were analyzed by Fourier transform infrared spectroscopy (FT-IR) with Nicolet iS10 infrared spectrometer. The samples were analyzed by X-ray photoelectron spectroscopy (XPS) with Thermo ESCALAB XI+ photoelectron spectrometer. All electrochemical tests were carried out using chi600e electrochemical workstation and traditional three electrode system, and the electrochemical experiments were carried out in phosphate buffer solution (PBS).

3. Results and discussion

3.1 Characterization of Cu/CuO/ZnO/PPy wire

The size and morphology of the prepared samples were characterized by scanning electron microscope. It can be seen that the surface of the oxi-

dized copper wire is uniform (**Figure 1A**), and the needle like CuO nanowires grow uniformly on the surface (**Figure 1B**). As shown in **Figure 1C**, the height of CuO nanowires is about $3 \mu\text{m}$. The average diameter is about 80 nm. The distribution of nanowires is relatively dispersed, which provides a good anchor for ZnO growth. As can be seen from **Figures 1D** and **1E**, the diameter is about $1 \mu\text{m}$ ZnO microspheres are uniformly covered on the surface of cu/cuo wire. High power scanning electron microscope images showed that CuO nanowires were inserted into ZnO microspheres to form a ball club structure (**Figure 1F**), indicating a strong p-n junction contact. After further modification with PPy, the outline of the microspheres can still be seen (**Figure 1G**), indicating that the PPy film is thin and uniform. The modified PPy film darkens the surface of the actual wire sample (**Figure 1H**). The prepared Cu/CuO/ZnO/PPy wire can be divided into three layers (**Figure 1I**): the inner Cu wire is used as the current transmission channel, the middle barrier layer (CuO/ZnO) is used as the driving factor, and the outer PPy film is used as the adsorption layer. The parsed structure is shown in **Figure 1J**.

In the XRD spectrum (**Figure 2A**), a series of peaks corresponding to Cu (JCPDS card No. 04-0836), ZnO crystalline phase (JCPDS card No. 36-1451) and CuO crystalline phase (JCPDS card No. 48-1548) can be observed. Because CuO has less components, its diffraction peak intensity is weaker than that of ZnO. It can be seen from the infrared spectrum (**Figure 2B**) that PPy exists in the proof materials of the absorption peaks of $1,540$ and $1,440 \text{ cm}^{-1}$ (C-C telescopic vibration), $1,169 \text{ cm}^{-1}$ (C-H deformation in the plane), $1,035 \text{ cm}^{-1}$ (N-H deformation in the plane), $2,925 \text{ cm}^{-1}$ (C-H telescopic vibration) and 890 cm^{-1} (C-H deformation out of the plane)^[28,29]. At $3,500$ and $1,640 \text{ cm}^{-1}$ (The absorption peak of δ OH (vibration) indicates the presence of adsorbed water^[30]; the absorption peak at 440 cm^{-1} belongs to Zn-O bond^[31]; the absorption peaks at 508 and 615 cm^{-1} belong to the Cu-O bond^[32].

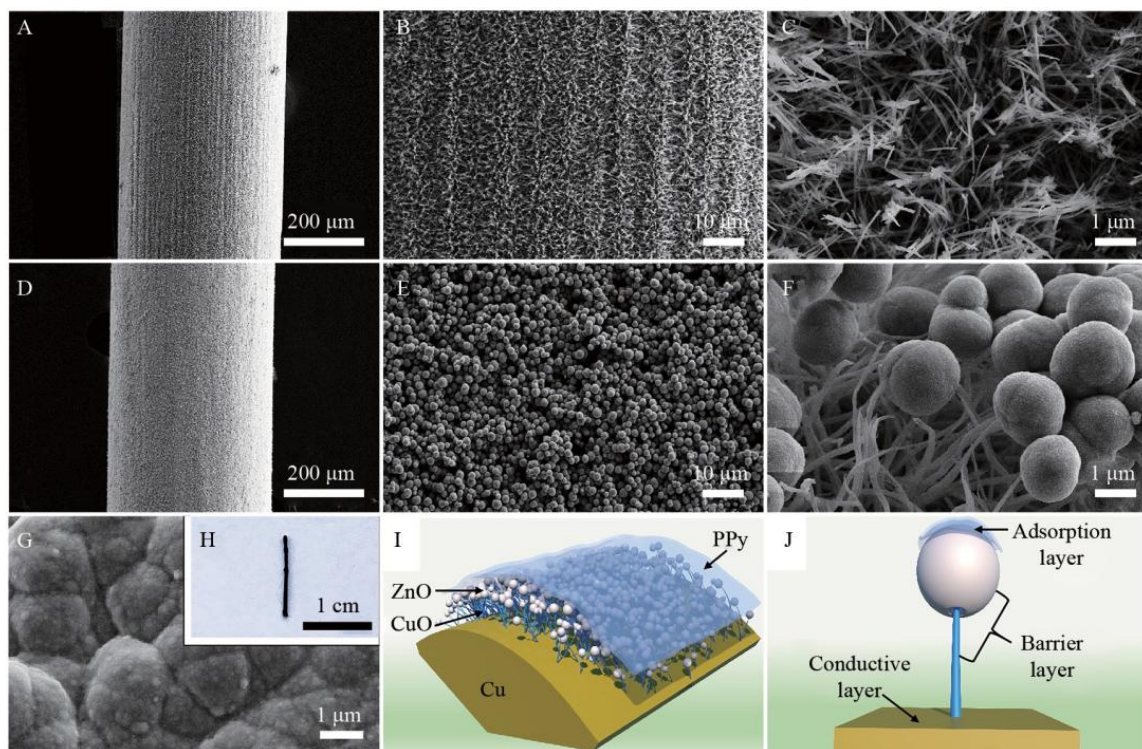


Figure 1. Scanning electron microscopy (SEM) images of the surface of the prepared Cu/CuO wire (A–C), Cu/CuO/ZnO wire (D–F) and Cu/CuO/ZnO/polypyrrole (PPy) wire (G); (H) photograph of the prepared Cu/CuO/ZnO/PPy wire; (I) schematic diagram of the Cu/CuO/ZnO/PPy wire; (J) schematic diagram of the local specific structure.

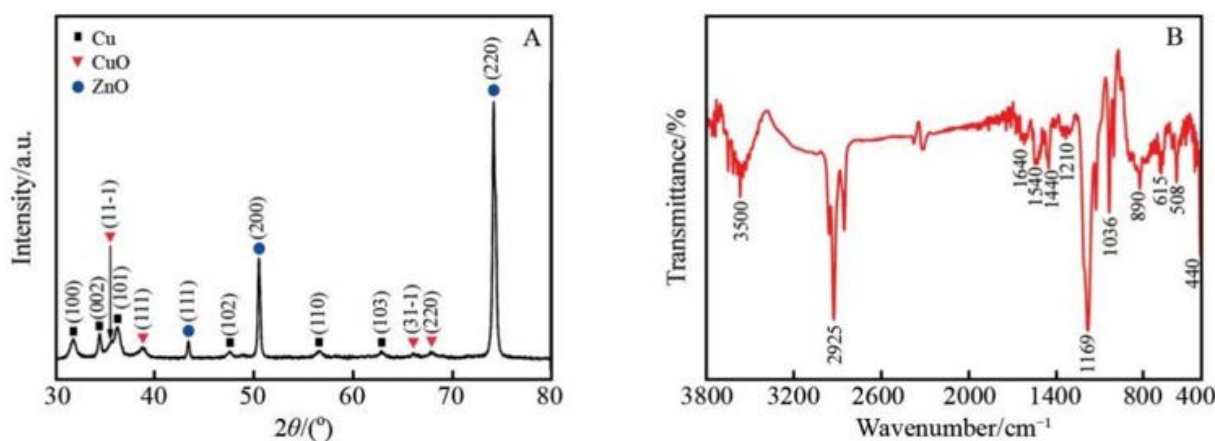


Figure 2. (A) X-ray diffraction (XRD) pattern of the Cu/CuO/ZnO wire; (B) fourier transform infrared (FTIR) spectrum of Cu/CuO/ZnO/PPy wire.

The elemental composition and oxidation state of Cu/CuO/ZnO wire were further characterized by XPS. XPS analysis spectrum showed that there were elements Cu, O and Zn in the material (**Figure 3**). The two signal peaks of Cu $2p^{3/2}$ and Cu $2p^{1/2}$ are 933.6 and 953.4 eV respectively, and the energy interval is 19.8 eV. The peaks of 941.4 and 961.5 eV are strong satellite peaks, indicating that the

component is CuO, not Cu_2O ^[33]. The O 1s spectrum consists of the signal peak of lattice oxygen at 530 eV and the signal peak of oxygen vacancy at about 531 eV^[33,34]. In addition, the Zn 2p spectrum consists of two kinds of orbitals of Zn^{2+} , including Zn $2p^{3/2}$ orbitals at 1021.8 eV and Zn $2p^{1/2}$ orbitals at 1044.8 eV^[35].

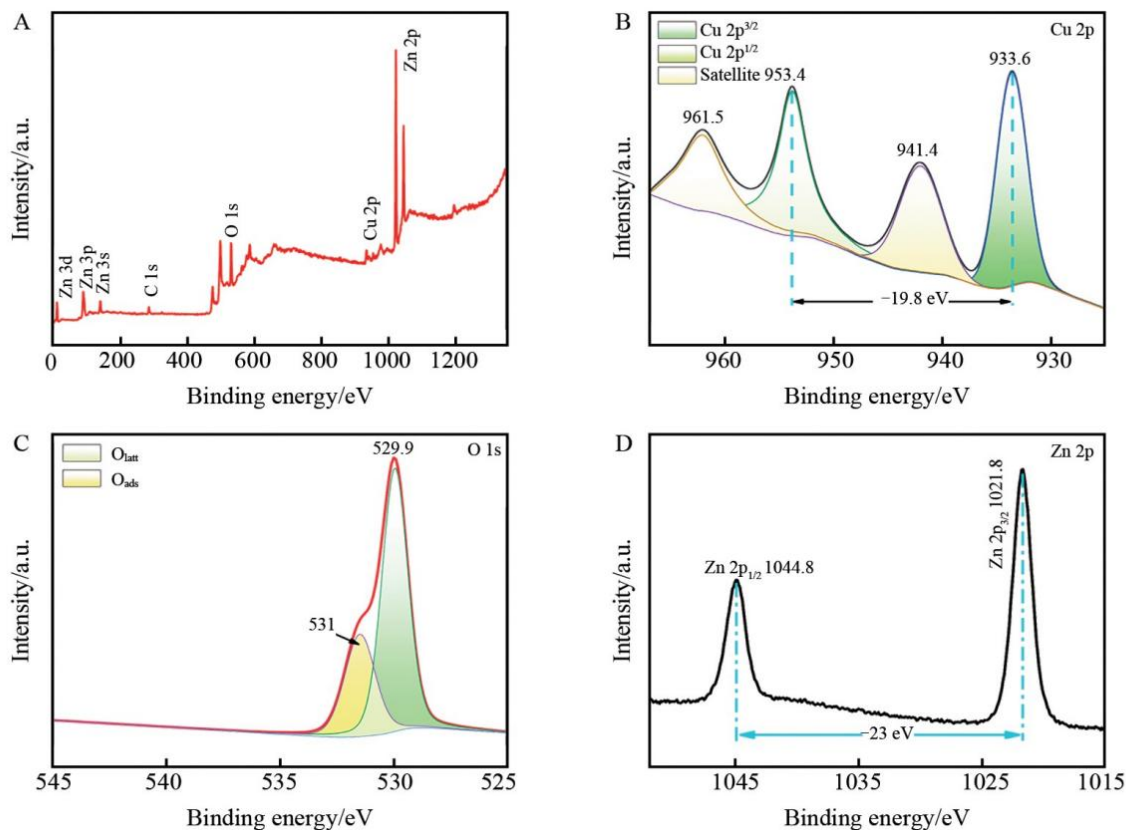


Figure 3. (A) XPS survey spectra of Cu/CuO/ZnO wire; (B) Cu 2p; (C) O 1s; (D) Zn 2p spectra.

3.2 Detection mechanism

The sensing mechanism of Cu/CuO/ZnO/PPy wire is shown in **Figure 4**. There is an interface potential barrier at the interface between p-type CuO and n-type ZnO. Because the p-n junction barrier hinders the transmission of electrons from ZnO to CuO, the change of barrier height will affect the electrochemical impedance, and then produce the corresponding electrochemical response. When Hg^{2+} appears near Cu/CuO/ZnO/PPy wire, due to the high affinity of NH functional group for Hg^{2+} (**Figure 4A**), Hg^{2+} coordinates with lone pair electrons on nitrogen and forms a stable complex, which is adsorbed on PPy^[36]. The positively charged PPy layer formed by adsorbing Hg^{2+} obtains electrons from ZnO, causing its conduction band to rise (**Figure 4B**). Since PPy cannot contact CuO, its energy band remains unchanged.

The adsorption of Hg^{2+} leads to the decrease of interface barrier (from Φ reach Φ') (**Figure 4C**). The decrease of electrochemical barrier will lead to the decrease of electrochemical impedance and the increase of current. The more Hg^{2+} adsorbed, the smaller the potential barrier, and the greater the current. Based on this, the direct detection of Hg^{2+} can be realized. The above theory is verified by the comparative experiment of differential pulse voltammetry (DPV). As shown in **Figure 5A**, when 500 nmol/L Hg^{2+} is added, the oxidation peak current of Cu/CuO/ZnO/PPy wire is significantly increased by about 112 μA . The current response produced by Cu/CuO/PPy wire and Cu/CuO/PPy wire is very low (**Figures 5B** and **5C**). The above results show that the interface effect of CuO/ZnO p-n junction is the main reason for the electrochemical response.

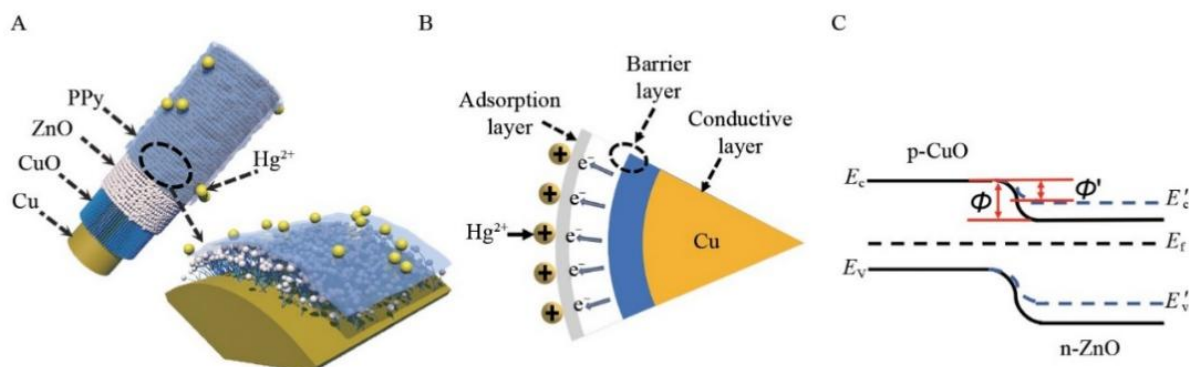


Figure 4. (A) schematic diagram of Cu/CuO/ZnO/PPy wire; (B) sectional view of 1/4 Cu/CuO/ZnO/PPy wire; (C) schematic diagram of energy bands and interface barrier adjustment at the p-n junction interface.

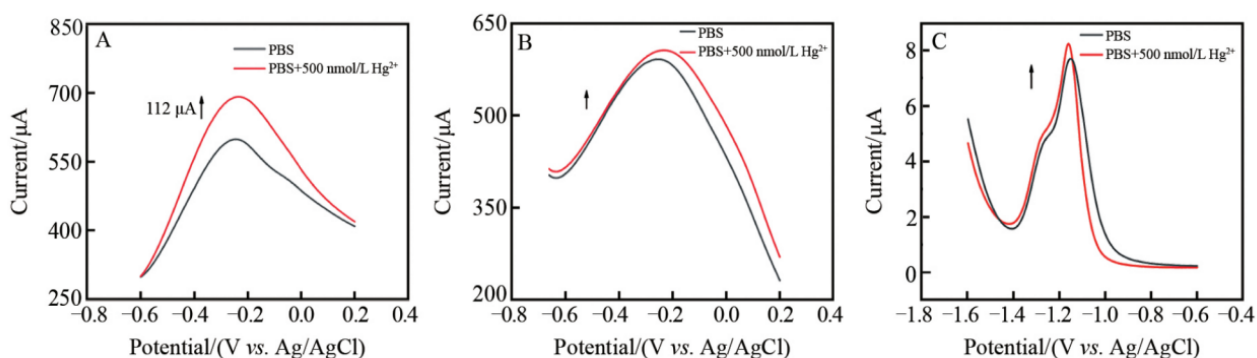


Figure 5. Differential pulse voltammetry (DPV) curves of Cu/CuO/ZnO/PPy wire (A), Cu/CuO/PPy wire (B) and Cu/ZnO/PPy wire (C) in the presence of 500 nmol/L Hg^{2+} .

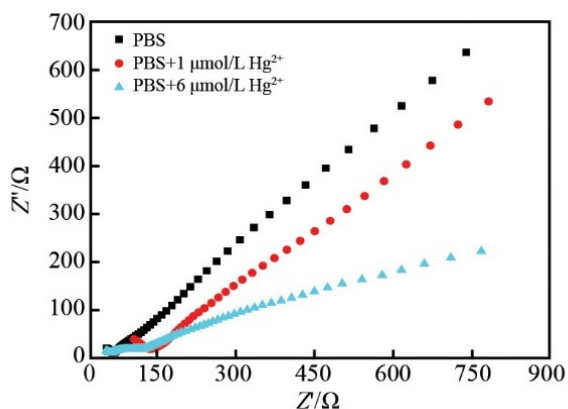


Figure 6. Nyquist plots of Cu/CuO/ZnO/PPy wire in the presence of Hg^{2+} in the frequency range from 0.01 Hz to 100 kHz.

The experimental results were verified by electrochemical impedance spectroscopy (EIS). As shown in **Figure 6**, the impedance of Cu/CuO/ZnO/PPy wire decreases with the increase of Hg^{2+} concentration. The results show that the change of electrochemical response is due to the

impedance change of heterojunction induced by Hg^{2+} .

3.3 Electrochemical detection of Hg^{2+}

The sensing performance of Cu/CuO/ZnO/PPy wire for Hg^{2+} was further studied. As shown in **Figure 7A**, in the range of 200–1600 nmol/L, the DPV response current increases proportionally with the increase of Hg^{2+} concentration. As shown in **Figure 7B**, there is a good linear relationship between DPV signal and the logarithm of Hg^{2+} concentration between 200–1600 nmol/L, and the linear regression equation is $I_{\text{Hg}}(\text{A}) = 158.37 \times \lg C(\text{nmol/L}) + 257.67$ ($R^2 = 0.98843$). Detection limit (LOD, 3σ) can be low to 2.1 pmol/L. The sensitivity is $1010.82 \mu\text{A} \cdot \text{L}/(\text{nmol} \cdot \text{cm}^2)$, higher than the results reported in the relevant literature (**Table 1**).

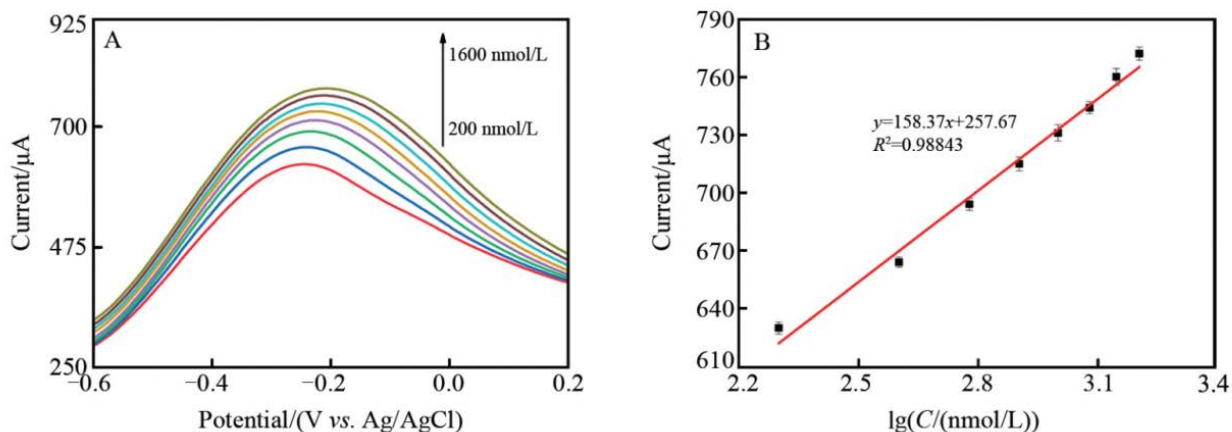


Figure 7. (A) DPV curves of Cu/CuO/ZnO/PPy wire toward different concentrations of Hg²⁺ in phosphate buffer solution (PBS, pH = 7.0); (B) Calibration curve of logarithm of Hg²⁺ concentration with DPV current.

Table 1. Sensing performance of various materials to Hg²⁺

Electrodes	Linear range (nmol /L)	Detection limit (nmol /L)	Sensitivity (μA·L / (nmol·cm ²))	Ref
Gold-nanoparticle/graphene	0.0395–0.25	0.0299	0.0354	[37]
DNA and a molecular light switch	1–150	0.35	-	[38]
CeO ₂ -RGO/GCE	2–120	0.0218	0.1035	[39]
3D-rGO/PANI	0.01–100	0.035	0.07216	[40]
Cu/Co	250–2,500	80	0.375	[41]
PPy-RGO/GCE	0–100	12	0.124	[42]
ZE-2	500–3,500	1.28	-	[43]
Ag/Au	0.03–1.5	0.0036	-	[44]
CoS _x /CdS	0.01–1,000	0.002	-	[45]
LI-MS-G@ ITO	5–5,000	2	-	[46]
Cu/CuO/ZnO/PPy wire	200–1,600	0.0021	1,010.82	This work

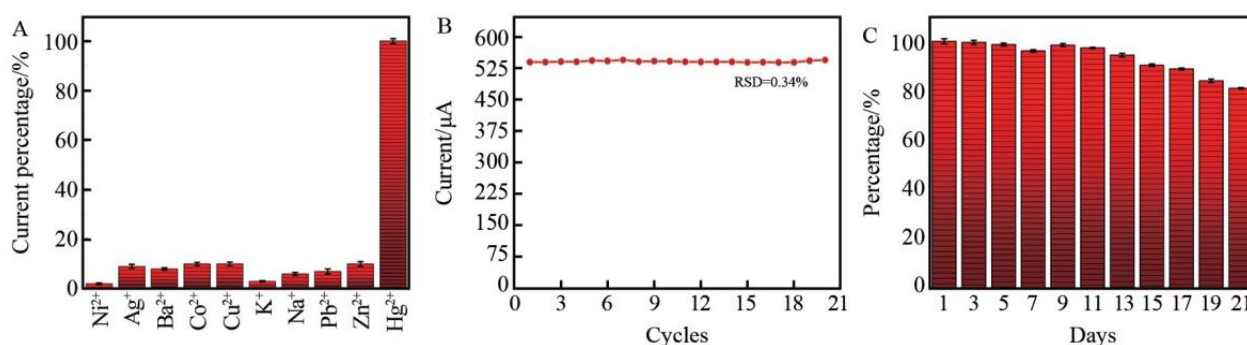


Figure 8. (A) Electrochemical current response of Cu/CuO/ZnO/PPy wire to 400 nmol/L Hg²⁺ and other interfering ions; (B) response to 200 nmol/L Hg²⁺ for repeated 20 times through a continuous cycle of the Cu/CuO/ZnO/PPy wire; (C) storage stability of Cu/CuO/ZnO/PPy wires evaluated by measuring the DPV response to 200 nmol/L Hg²⁺ every two days for 21 days.

The selectivity of Cu/CuO/ZnO/PPy wire to Hg²⁺ was investigated by adding a variety of other metal ions with the same concentration. It can be seen from **Figure 8A** that when the concentration of all metal ions is 400 nmol/L, the electrochemical response of the composite to Hg²⁺ is much greater than that of other metal ions, indicating that it has

good anti-interference ability. Because polypyrrole can selectively adsorb Hg²⁺, it can change the level of interface barrier, and then change the electrochemical response. Other ions are shielded by PPy, which cannot change the height of the interface barrier through physical effects, so it cannot change the electrochemical response. Therefore, this sensing

mechanism can distinguish target ions well and has good selectivity. As shown in **Figure 8B**, 20 DPV cycles were carried out after adding 200 nmol/L Hg^{2+} , and the relative standard deviation (RSD) was 0.3%, indicating that Cu/CuO/ZnO/PPy wire had good stability and reproducibility. The DPV response current of 200 nmol/L Hg^{2+} was measured every two days for 21 consecutive days to investigate its long-term stability. After the 21st day, it still maintained 81% of the initial electrochemical response strength (**Figure 8C**), indicating that Cu/CuO/ZnO/PPy wire has good long-term stability.

3.4 Detection of Hg^{2+} in actual water samples

This method is used to detect Hg^{2+} in tap water, river water and sea water to verify the practicability of Cu/CuO/ZnO/PPy wire. As shown in **Table 2**, at the addition levels of 100 and 500 nmol/L, the recovery of Hg^{2+} is 97.3%–105.0%, and the RSD is 1.8%–5.6%. The results show that Cu/CuO/ZnO/PPy wire has good practicability for the detection of Hg^{2+} in actual water samples.

Table 2. Detection of Hg^{2+} in real water samples by the proposed sensor

Sample	Added (nmol/L)	Found (nmol/L)	Recovery (%)	RSD (% , n = 3)
Tap water	100	103.6	103.6	5.6
	500	486.3	97.3	5.4
River water	100	105.0	105.0	4.3
	500	512.4	102.5	4.9
Sea water	100	97.5	97.5	2.8
	500	510.5	102.1	1.8

4. Conclusion

Cu/CuO/ZnO/PPy wire was prepared and applied to the direct detection of Hg^{2+} in actual water samples. The p-n interface barrier is used as the driving factor of electrochemical response. This sensing method has high sensitivity ($1,010.82 \mu\text{A}\cdot\text{L}/(\text{nmol}\cdot\text{cm}^2)$), low LOD (2.1 pmol/L) and excellent selectivity. The recovery rate of Hg^{2+} in actual water samples is 97.3%–105.0%, which has a good application prospect. This method is simple, fast and intuitive, and is suitable for the on-site detection of Hg^{2+} . P-n junction barrier is expected to be applied to other heavy metal detection sen-

sors.

Acknowledgements

The project was funded by Fundamental Research Funds for Central Universities (Nos. 202042009, 201964011) and National Natural Science Foundation of China (No. 52072353).

Conflict of interest

The authors declared no conflict of interest.

References

- Li C, Niu Q, Wang J, *et al.* Bithiophene-based fluorescent sensor for highly sensitive and ultrarapid detection of Hg^{2+} in water, seafood, urine and live cells. *Spectrochim Acta Part A: Molecular and Biomolecular Spectroscopy* 2020; 233: 118–208.
- Counter SA, Buchanan LH. Mercury exposure in children: A review. *Toxicology and Applied Pharmacology* 2004; 198(2): 209–230.
- Li X, Du Z, Lin S, *et al.* Corrigendum to “ExoIII and TdT dependent isothermal amplification (ETDA) colorimetric biosensor for ultra-sensitive detection of Hg^{2+} ”. *Food Chemistry* 2020; 316: 126303.
- Zhang H, Lei Z, Fu X, *et al.* Hg^{2+} -triggered exonuclease III-assisted dual-cycle targets recycling amplification for label-free and ultrasensitive colorimetric detection of Hg^{2+} . *Sensors and Actuators B: Chemical* 2017; 246: 896–903.
- Zhang M, Ge L, Ge S, *et al.* Three-dimensional paper-based electrochemiluminescence device for simultaneous detection of Pb^{2+} and Hg^{2+} based on potential-control technique. *Biosensors and Bioelectronics* 2013; 41: 544–550.
- Li Z, Miao X, Xing K, *et al.* Ultrasensitive electrochemical sensor for Hg^{2+} by using hybridization chain reaction coupled with Ag@ Au core-shell nanoparticles. *Biosensors and Bioelectronics* 2016; 80: 339–343.
- Wang N, Lin M, Dai H, *et al.* Functionalized gold nanoparticles/reduced graphene oxide nanocomposites for ultrasensitive electrochemical sensing of mercury ions based on thymine–mercury–thymine structure. *Biosensors and Bioelectronics* 2016; 79: 320–326.
- Zhuang Y, Zhao M, He Y, *et al.* Fabrication of ZnO/rGO/PPy heterostructure for electrochemical detection of mercury ion. *Journal of Electroanalytical Chemistry* 2018; 826: 90–95.
- Chaivo S, Chailapakul O, Siangproh W. Highly sensitive determination of mercury using copper enhancer by diamond electrode coupled with sequential injection–anodic stripping voltammetry. *Analytica Chimica Acta* 2014; 852: 55–62.
- Cui L, Wu J, Ju H. Electrochemical sensing of heavy metal ions with inorganic, organic and bio-materials.

- Biosensors and Bioelectronics 2015; 63: 276–286.
11. Syshchik O, Skypyshevsky VA, Soldatkin OO, *et al.* Enzyme biosensor systems based on porous silicon photoluminescence for detection of glucose, urea and heavy metals. *Biosensors and Bioelectronics* 2015; 66: 89–94.
 12. Martiniano LC, Abrantes VR, Neto SY, *et al.* Direct simultaneous determination of Pb (II) and Cu (II) in biodiesel by anodic stripping voltammetry at a mercury-film electrode using microemulsions. *Fuel* 2013; 103: 1164–1167.
 13. Jia J, Du X, Zhang Q, *et al.* Z-scheme MgFe₂O₄/Bi₂MoO₆ heterojunction photocatalyst with enhanced visible light photocatalytic activity for malachite green removal. *Applied Surface Science* 2019; 492: 527–539.
 14. Jiang Y, Liao J, Chen H, *et al.* All-solid-state Z-scheme α -Fe₂O₃/amine-RGO/CsPbBr₃ hybrids for visible-light-driven photocatalytic CO₂ reduction. *Chem* 2020; 6(3): 766–780.
 15. Daemi S, Ghasem IS, Ashkarran AA. Electrospun CuO-ZnO nanohybrid: Tuning the nanostructure for improved amperometric detection of hydrogen peroxide as a non-enzymatic sensor. *Journal of Colloid and Interface Science* 2019; 550: 180–189.
 16. Wang L, Tahir M, Chen H, *et al.* Probing charge carrier transport and recombination pathways in monolayer MoS₂/WS₂ heterojunction photoelectrodes. *Nano Letters* 2019; 19(12): 9084–9094.
 17. Qiao S, Zhao J, Zhang B, *et al.* Micrometer-Scale biomass carbon tube matrix auxiliary MoS₂ heterojunction for electrocatalytic hydrogen evolution. *International Journal of Hydrogen Energy* 2019; 44(60): 32019–32029.
 18. Shang J, Zhao M, Qu H, *et al.* New application of pn junction in electrochemical detection: The detection of heavy metal ions. *Journal of Electroanalytical Chemistry* 2019; 855: 113624.
 19. Gai P, Yu W, Zhao H, *et al.* Solar-powered organic semiconductor-bacteria biohybrids for CO₂ reduction into acetic acid. *Angewandte Chemie International Edition* 2020; 59: 7224–7229.
 20. Zhao M, Shang J, Qu H, *et al.* Fabrication of the Ni/ZnO/BiOI foam for the improved electrochemical biosensing performance to glucose. *Analytica Chimica Acta* 2019; 1095: 93–98.
 21. Singh J, Soni RK. Controlled synthesis of CuO decorated defect enriched ZnO nanoflakes for improved sunlight-induced photocatalytic degradation of organic pollutants. *Applied Surface Science* 2020; 521: 146420.
 22. Kaviyarasu K, Magdalane CM, Anand K, *et al.* Synthesis and characterization studies of MgO: CuO nanocrystals by wet-chemical method. *Spectrochimica Acta Part A: Molecular and Biomolecular Spectroscopy* 2015; 142: 405–409.
 23. Aneesiya KR, Louis C. Localized surface plasmon resonance of Cu-doped ZnO nanostructures and the material's integration in dye sensitized solar cells (DSSCs) enabling high open-circuit potentials. *Journal of Alloys and Compounds* 2020; 829: 154497.
 24. Xia W, Wang Y, Wang Q, *et al.* Tubular acceptor-rich ZnO hierarchical heterostructure as an efficient photocatalyst for organic degradation. *Applied Surface Science* 2019; 506: 145008.
 25. Rezaei B, Boroujeni MK, Ensafi AA. Caffeine electrochemical sensor using imprinted film as recognition element based on polypyrrole, sol-gel, and gold nanoparticles hybrid nanocomposite modified pencil graphite electrode. *Biosensors and Bioelectronics* 2014; 60: 77–83.
 26. Chandra V, Kim KS. Highly selective adsorption of Hg²⁺ by a polypyrrole-reduced graphene oxide composite. *Chemical Communications* 2011; 47(13): 3942–3944.
 27. Khanna PK, Bhanot S, Dhanwe V, *et al.* In situ SeO₂ promoted synthesis of CdSe/PPy and Se/PPy nanocomposites and their utility in optical sensing for detection of Hg²⁺ ions. *RSC Advances* 2015; 5(113): 92818–92828.
 28. Jafarian M, Afghahi SSS, Atassi Y, *et al.* Promoting the microwave absorption characteristics in the X band using core-shell structures of Cu metal particles/PPy and hexaferrite/PPy. *Journal of Magnetism and Magnetic Materials* 2019; 493: 165680.
 29. Olad A, Rashidzadeh A, Amini M. Preparation of polypyrrole nanocomposites with organophilic and hydrophilic montmorillonite and investigation of their corrosion protection on iron. *Advances in Polymer Technology* 2013; 32(2): 21337.
 30. Noei H, Qiu H, Wang Y, *et al.* The identification of hydroxyl groups on ZnO nanoparticles by infrared spectroscopy. *Physical Chemistry Chemical Physics* 2008; 10(47): 7092–7097.
 31. Huang J, Yang Z, Yang B, *et al.* Ultrasound assisted polymerization for synthesis of ZnO/Polypyrrole composites for zinc/nickel rechargeable battery. *Journal of Power Sources* 2014; 271: 143–151.
 32. Yin Z, Fan W, Ding Y, *et al.* Shell structure control of PPy-modified CuO composite nanoleaves for lithium batteries with improved cyclic performance. *ACS Sustainable Chemistry & Engineering* 2015; 3(3): 507–517.
 33. Wang W, Xu L, Zhang R, *et al.* Coexistence of ferromagnetism and paramagnetism in ZnO/CuO nanocomposites. *Chemical Physics Letters* 2019; 721: 57–61.
 34. Xu L, Zhou Y, Wu Z, *et al.* Improved photocatalytic activity of nanocrystalline ZnO by coupling with CuO. *Journal of Physics and Chemistry of Solids* 2017; 106: 29–36.
 35. Li B, Wang Y. Facile synthesis and photocatalytic activity of ZnO–CuO nanocomposite. *Superlattices and Microstructures* 2010; 47(5): 615–623.
 36. Chandra V, Kim KS. Highly selective adsorption of Hg²⁺ by a polypyrrole-reduced graphene oxide composite. *Chemical Communications* 2011; 47(13): 3942–3944.
 37. Gong JM, Zhou T, Song DD, *et al.* Monodispersed

- Au nanoparticles decorated graphene as an enhanced sensing platform for ultrasensitive stripping voltammetric detection of mercury (II). *Sensors and Actuators B: Chemical* 2010; 150(2): 491–497.
38. Zhang X, Li Y, Su H, *et al.* Highly sensitive and selective detection of Hg²⁺ using mismatched DNA and a molecular light switch complex in aqueous solution. *Biosensors and Bioelectronics* 2010; 25(6): 1338–1343.
 39. Xie Y, Zhao S, Ye H, *et al.* Graphene/CeO₂ hybrid materials for the simultaneous electrochemical detection of cadmium (II), lead (II), copper (II), and mercury (II). *Journal of Electroanalytical Chemistry* 2015; 757: 235–242.
 40. Wen G, Zhao W, Chen X, *et al.* N-doped reduced graphene oxide/MnO₂ nanocomposite for electrochemical detection of Hg²⁺ by square wave stripping voltammetry. *Electrochimica Acta* 2018; 291: 95–102.
 41. Sharma VV, Tonelli D, Guadagnini L, *et al.* Copper-cobalt hexacyanoferrate modified glassy carbon electrode for an indirect electrochemical determination of mercury. *Sensors and Actuators B: Chemical* 2017; 238: 9–15.
 42. Zhao Z, Chen X, Yang Q, *et al.* Selective adsorption toward toxic metal ions results in selective response: Electrochemical studies on a polypyrrole/reduced graphene oxide nanocomposite. *Chemical Communications* 2012; 48(16): 2180–2182.
 43. Ma L, Zhang X, Ikram M, *et al.* Controllable synthesis of an intercalated ZIF-67/EG structure for the detection of ultratrace Cd²⁺, Cu²⁺, Hg²⁺ and Pb²⁺ ions. *Chemical Engineering Journal* 2020; 395: 125216.
 44. Li Z, Miao X, Xing K, *et al.* Ultrasensitive electrochemical sensor for Hg²⁺ by using hybridization chain reaction coupled with Ag@ Au core-shell nanoparticles. *Biosensors and Bioelectronics* 2016; 80: 339–343.
 45. Zhang L, Feng L, Li P, *et al.* Direct Z-scheme photocatalyst of hollow CoS_x@ CdS polyhedron constructed by ZIF-67-templated one-pot solvothermal route: A signal-on photoelectrochemical sensor for mercury (II). *Chemical Engineering Journal* 2020; 395: 125072.
 46. Ge L, Hong Q, Li H, *et al.* Direct-laser-writing of metal sulfide-graphene nanocomposite photoelectrode toward sensitive photoelectrochemical sensing. *Advanced Functional Materials* 2019, 29(38): 1904000.